Indoor MIMO Channels: A Parametric Correlation Model and Experimental Results

Shuangquan Wang*, Kaustubha Raghukumar†, Ali Abdi*, Jon Wallace‡, Michael Jensen‡

*New Jersey Center for Wireless Telecommunications and Center for Communications and Signal Processing Research
Department of Electrical and Computer Engineering
New Jersey Institute of Technology, Newark, NJ 07102 Email: {sw27,ali.abdi}@njit.edu
†Marine Physical Laboratory, Scripps Institution of Oceanography
Univ. of California at San Diego, San Diego, CA 92093 Email: kaus@mpl.ucsd.edu
‡Department of Electrical and Computer Engineering
Brigham Young University, Provo, Utah 84602 Email: wall@ieee.org, jensen@ee.byu.edu

***Abstract*— Accurate modeling of indoor multiple-input multiple-output (MIMO) channels is an important prerequisite for multi-antenna system design. In this paper, a new model for indoor MIMO channels is proposed, and a closed-form expression for the spatio-temporal cross-correlation function between any two subchannels is derived. This new analytical correlation expression includes many key physical parameters of interest such as mean angle-of-departure at the transmitter and mean angle-of-arrival at the receiver, the associated angle spreads, the distance between transmitter and receiver, etc., in a compact form. Comparison of this model with channel correlations and capacity, using the collected indoor MIMO data, exhibits the utility of the model.**

I. Introduction

The utilization of antenna arrays at the base station (BS) and the mobile station (MS) in a wireless communication system leads to a form of spatial diversity that can result in a significant increase in achievable capacity. This capacity has been shown to increase with the number of spatial subchannels between the transmitter and receiver, provided that the environment is sufficiently rich in multi-path components [1]. This gives rise to the need for accurate channel models that can sufficiently capture various parameters of a multiple-input multiple-output (MIMO) environment, facilitating the decision making for system design.

An important aspect of MIMO channels is the cross-correlation between the various elements of the channel matrix. Currently, a popular correlation model makes use of the separability argument between the transmitter and receiver, which entails modeling the transmit and receive correlation matrices separately, and then finding the product of the two in order to obtain the final correlation matrix. See [2] and [3] and references therein for further information. However, the explicit connection between the elements of such a channel correlation matrix and the physical characteristics of the channel such as the mean angle-of-arrival (AoA) and angle-of-departure (AoD), the associated angle spreads, etc., are not clear. On the other hand, it is important for the system designer to know how the correlation matrix is affected as the parameters of the channel change. This contribution proposes a joint correlation model which takes into account the distribution of the scatterers at each end of the radio communication link and the parameters associated with such distributions.

A physical model has been recently proposed for outdoor MIMO channels [4] with the advantage of having a closed form expression for MIMO spatio-temporal cross-correlation (STCC). In order to come up with a mathematically tractable indoor correlation model, much needed for analytical calculations and system design, we extend the model of [4] in several ways. The measurement data collected at Brigham Young University [5] is used to evaluate the accuracy of the new model.

The rest of the paper is organized as follows. The proposed two-ring model for indoors is presented in Section II, whereas a compact result for the STCC function between any two subchannels is derived in Section III. In Section IV we compare the proposed model with measured data. Concluding remarks are given in Section V.

II. The Two-Ring Model

The proposed model is shown in Fig. 1, where the scatterers local to BS and MS are modeled to be distributed on two separate rings. The main difference between our model and other two-ring models [6][7] is that we consider single-bounce scatterings only, conceptually consistent with [8], which allows us to obtain closed form and mathematically tractable results.

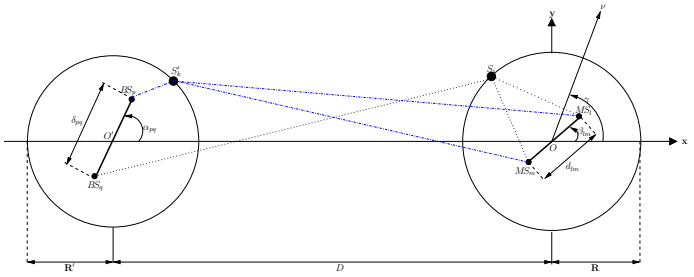

Fig. 1. Geometrical configuration of a 2×2 channel with local scatterers around the MS and BS, with single-bounce rays shown in the forward channel

Now we proceed to discuss the analytical framework for derivation of the MIMO STCC function for our two-ring model.

According to Fig. 1, in the forward channel, the MS receives single-bounce rays from scatterer S_i around the MS (shown in Fig. 1 by dotted lines) and scatterer S'_k around the BS (shown in Fig. 1 by dash-dotted lines). D is the distance between the MS and BS, while R and R' are the radii of the rings of scatterers around the MS and BS, respectively, whereas α_{pq} and β_{lm} are the directions of BS and MS arrays, respectively. For the frequency non-selective communication link between the the element BS_p and the element MS_l (the forward channel), let $h_{lp}(t)$ denote the complex low-pass equivalent channel gain. Mathematical representation of the superposition of rays at the MS results in the following expression for the channel gain

$$h_{lp}(t)=\sqrt{\eta'\Omega_{lp}}\lim_{N'\to\infty}\frac{1}{\sqrt{N'}}\sum_{k=1}^{N'}g'_k\exp\{j\psi'_k-\frac{j2\pi}{\lambda}(\xi'_{pk}+\xi'_{kl})+j2\pi f_d\cos(\varphi'_k-\gamma)t\}+\sqrt{\eta\Omega_{lp}}\lim_{N\to\infty}\frac{1}{\sqrt{N}}\sum_{i=1}^{N}g_i\times\exp\{j\psi_i-\frac{j2\pi}{\lambda}(\xi_{pi}+\xi_{il})+j2\pi f_d\cos(\phi_i-\gamma)t\}. \quad (1)$$

In Eq. (1), Ω_{lp} is the power transmitted through the BS_p-MS_l link, i.e., $\Omega_{lp}=E[|h_{lp}|^2]\leq 1$, whereas η' and η show the contributions of BS and MS rings to Ω_{lp} such that $\eta'+\eta=1$, N and N' are the number of independent scatterers around the MS and BS, respectively, the positive variables g_i and g'_k represent the amplitudes of the waves scattered by the S_i and S'_k, respectively, ψ_i and ψ'_k are the associated phase shifts, and ξ's and ξ''s are the distances shown in Fig. 2, φ_i and ϕ'_k are the AoD of the waves traveling from the BS, and ϕ_i and φ'_k are the AoA of the waves toward the MS. The sets $\{g_i\}_{i=1}^{\infty}$ and $\{g'_k\}_{k=1}^{\infty}$ consist of independent positive random variables with finite variances, independent of $\{\psi_i\}_{i=1}^{\infty}$ and $\{\psi'_k\}_{k=1}^{\infty}$. We assume that $\{\psi_i\}_{i=1}^{\infty}$ and $\{\psi'_k\}_{k=1}^{\infty}$ are uniform and i.i.d random variables with uniform distributions over $[0,2\pi)$. We also set $N^{-1}\sum_{i=1}^{N}E[g_i^2]=1$ and $N'^{-1}\sum_{k=1}^{N'}E[g_k'^2]=1$ which result in the desired identity $E[|\ h_{lp}(t)\ |^2]=\Omega_{lp}$.

III. The MIMO Correlation

Based on the statistical properties of $\{g_i\}_{i=1}^{\infty}$, $\{g'_k\}_{k=1}^{\infty}$, $\{\psi_i\}_{i=1}^{\infty}$ and $\{\psi'_k\}_{k=1}^{\infty}$, the normalized STCC between the two subchannel gains $h_{lp}(t)$ and $h_{mq}(t)$, defined as $\rho_{lp,mq}(\tau)=E[h_{lp}(t)h^*_{mq}(t+\tau)]/(\Omega_{lp}\Omega_{mq})^{1/2}$, can be written as the following form:

$$\rho_{lp,mq}(\tau)=\lim_{N'\to\infty}\frac{(1-\eta)}{N'}\sum_{k=1}^{N'}E[g_k'^2]\exp\Big\{-j\frac{2\pi}{\lambda}(\xi'_{pk}-\xi'_{qk}+\xi'_{kl}-\xi'_{km})-j2\pi f_d\cos(\varphi'_k-\gamma)\tau\Big\}+\lim_{N\to\infty}\frac{\eta}{N}\sum_{i=1}^{N}E[g_i^2]\exp\Big\{-j\frac{2\pi}{\lambda}(\xi_{pi}-\xi_{qi}+\xi_{il}-\xi_{im})-j2\pi f_d\cos(\phi_i-\gamma)\tau\Big\}. \quad (2)$$

For not so small N' and N, the small power contributions from S_i and S'_k, out of the total power Ω_{lp}, are proportional to $E[{g_i}^2]/N$ and $E[{g'_k}^2]/N'$ respectively. This is equal to the infinitesimal powers coming from the differential angles $d\phi$ and $d\phi'$ with probabilities $f_{MS}(\phi_i)d\phi$ and $f_{BS}(\phi'_k)d\phi'$, respectively, i.e. $\frac{1}{N}E[g_i^2]=f_{MS}(\phi_i)d\phi$ and $\frac{1}{N'}E[g_k'^2]=f_{BS}(\phi'_k)d\phi'$ (see p. 23 of [9]), where $f_{MS}(\cdot)$ and $f_{BS}(\cdot)$ are the PDF's of the AoA and AoD of the MS and BS respectively. Then Eq. (2) can be represented by the following integral form:

$$\rho_{lp,mq}(\tau)=(1-\eta)\int_{-\pi}^{\pi}\exp\Big\{-\frac{j2\pi}{\lambda}(\xi'_{px}-\xi'_{qx}+\xi'_{xl}-\xi'_{xm})-j2\pi f_d\cos(\varphi'_x-\gamma)\tau\Big\}f_{BS}(x)dx+\eta\int_{-\pi}^{\pi}\exp\Big\{-\frac{j2\pi}{\lambda}(\xi_{py}-\xi_{qy}+\xi_{yl}-\xi_{ym})-j2\pi f_d\cos(y-\gamma)\tau\Big\}f_{MS}(y)dy, \quad (3)$$

where x and y denote respectively independent angular variables ϕ'_k and ϕ_i; Note that, for example, ξ'_{px} is the length of the path between the antenna element BS_p and the point on the ring of scatterers around the BS, determined by ϕ'_k, and so forth. For any given $f_{MS}(\cdot)$ and $f_{BS}(\cdot)$, Eq. (3) can be calculated numerically, according to the following relations, based on the application of the law of cosines in appropriate triangles in Fig. 2.

$$\begin{aligned}
\xi'^2_{px}&=(\delta^2_{pq}/4)+R'^2-\delta_{pq}R'\cos(\alpha_{pq}-x)\\
\xi'^2_{qx}&=(\delta^2_{pq}/4)+R'^2+\delta_{pq}R'\cos(\alpha_{pq}-x)\\
\xi'^2_{xl}&=(d^2_{lm}/4)+\xi'^2_x-\xi'_x d_{lm}\cos(v-\beta_{lm})\\
\xi'^2_{xm}&=(d^2_{lm}/4)+\xi'^2_x+\xi'_x d_{lm}\cos(v-\beta_{lm})\\
\xi^2_{py}&=(\delta^2_{pq}/4)+\xi^2_y-\xi_y\delta_{pq}\cos(\alpha_{pq}-w)\\
\xi^2_{qy}&=(\delta^2_{pq}/4)+\xi^2_y+\xi_y\delta_{pq}\cos(\alpha_{pq}-w)\\
\xi^2_{yl}&=(d^2_{lm}/4)+R^2-d_{lm}R\cos(y-\beta_{lm})\\
\xi^2_{ym}&=(d^2_{lm}/4)+R^2+d_{lm}R\cos(y-\beta_{lm}),
\end{aligned} \quad (4)$$

in which v and w denote φ'_k and φ_i, whereas ξ'_x and ξ_y are continuous versions of ξ'_k and ξ_i, shown in Fig. 2). Besides, for any given x, v and ξ'_x can be determined by the application of the law of sines to the triangle $O'S'_kO$

$$D/\sin(v-x)=R'/\sin(\pi-v)=\xi'_x/\sin(x). \quad (5)$$

In a similar manner, for a given y,w and ξ_y can be calculated by the application of the law of sines in the triangle $O'S_iO$

$$D/\sin(y-w)=R/\sin(w)=\xi_y/\sin(y). \quad (6)$$

The assumption $D\gg\max(R',R)\gg\max(\delta_{pq},d_{lm})$ is true in many practical cases of interest. We use the approximate relations $\sqrt{1+\chi}\approx 1+\chi/2$, $\sin(\chi)\approx\chi$ and $\cos(\chi)\approx 1$, when χ is small enough to simplify (4). To begin with, the first equation in (6) yields $w\approx\Delta\sin(y)$ as w and Δ are small, and the first equation in (5) yields $\pi-v\approx\Delta'\sin(x)$.

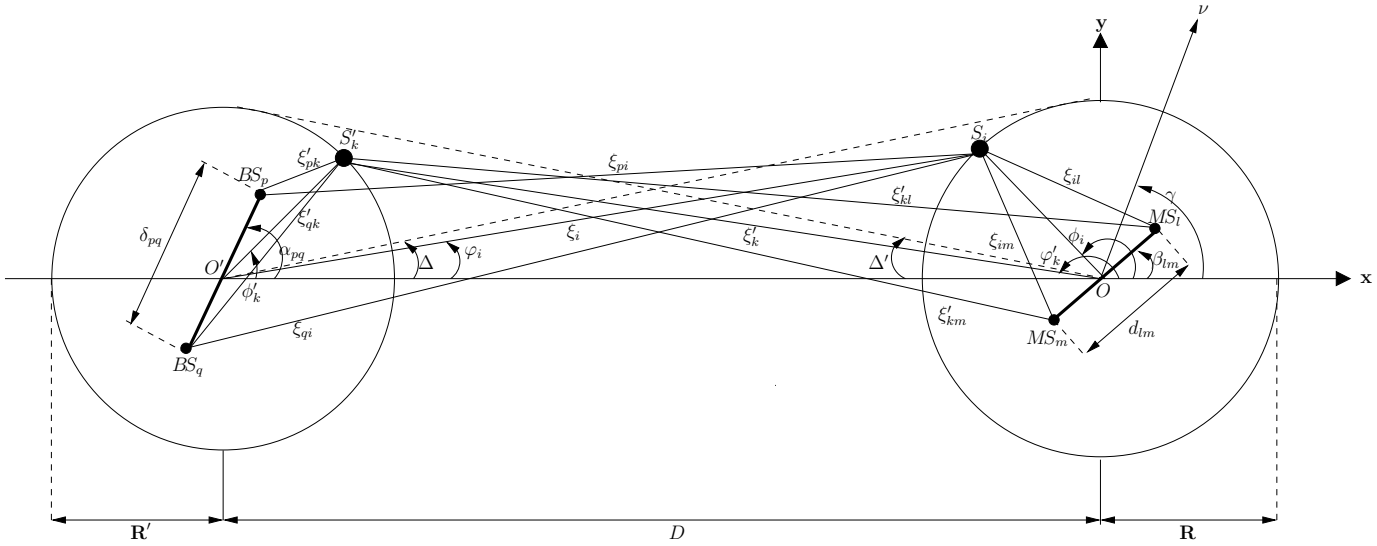

Fig. 2. Detailed version of Fig. 1

As a result, (4) can be written as:

$$\begin{aligned}
\xi_{px}' &\approx R' - (\delta_{pq}/2)\cos(\alpha_{pq} - x) \\
\xi_{qx}' &\approx R' + (\delta_{pq}/2)\cos(\alpha_{pq} - x) \\
\xi_{xl}' &\approx \xi_x' + (d_{lm}/2)[\cos(\beta_{lm}) - \Delta' \sin(\beta_{lm})\sin(x)] \\
\xi_{xm}' &\approx \xi_x' - (d_{lm}/2)[\cos(\beta_{lm}) - \Delta' \sin(\beta_{lm})\sin(x)] \\
\xi_{py} &\approx \xi_y - (\delta_{pq}/2)[\cos(\alpha_{pq}) + \Delta \sin(\alpha_{pq})\sin(y)] \\
\xi_{qy} &\approx \xi_y + (\delta_{pq}/2)[\cos(\alpha_{pq}) + \Delta \sin(\alpha_{pq})\sin(y)] \\
\xi_{yl} &\approx R - (d_{lm}/2)\cos(y - \beta_{lm}) \\
\xi_{ym} &\approx R + (d_{lm}/2)\cos(y - \beta_{lm}).
\end{aligned} \tag{7}$$

In this paper we consider two independent von Mises distributions for $f_{BS}(\cdot)$ and $f_{MS}(\cdot)$ (see [4] for the definition of von Mises distribution). This, together with (7), reduces the STCC function in (3) to the following key closed form expression:

$$\begin{aligned}
\rho_{lp,mq}(\tau) \approx (1-\eta)\frac{\exp\{-j[b_{lm}\cos(\beta_{lm}) - a\cos(\gamma)]\}}{I_0(\kappa')} \\
\times I_0\Big(\{\kappa'^2 - a^2\Delta'^2\sin^2\gamma - b_{lm}^2\Delta'^2\sin^2(\beta_{lm}) - c_{pq}^2 \\
- 2b_{lm}c_{pq}\Delta'\sin(\alpha_{pq})\sin(\beta_{lm}) + 2a\Delta'\sin(\gamma)[c_{pq}\sin(\alpha_{pq}) \\
+ b_{lm}\Delta'\sin(\beta_{lm})] - j2\kappa'[a\Delta'\sin(\mu')\sin(\gamma) - b_{lm}\Delta'\sin(\beta_{lm}) \\
\times \sin(\mu') - c_{pq}\cos(\alpha_{pq} - \mu')]\}^{1/2}\Big) + \eta\frac{\exp\{j[c_{pq}\cos(\alpha_{pq})]\}}{I_0(\kappa)} \\
\times I_0\Big(\{\kappa^2 - a^2 - b_{lm}^2 - c_{pq}^2\Delta^2\sin^2(\alpha_{pq}) + 2c_{pq}\Delta\sin(\alpha_{pq}) \\
\times [a\sin(\gamma) - b_{lm}\sin(\beta_{lm})] + 2ab_{lm}\cos(\beta_{lm} - \gamma) - j2\kappa[a\cos(\mu \\
- \gamma) - b_{lm}\cos(\beta_{lm} - \mu) - c_{pq}\Delta\sin(\alpha_{pq})\sin(\mu)]\}^{1/2}\Big),
\end{aligned} \tag{8}$$

where $a = 2\pi f_d \tau$, $b_{lm} = 2\pi d_{lm}/\lambda$, $c_{pq} = 2\pi\delta_{pq}/\lambda$, $I_0(\cdot)$ is the zeroth-order modified Bessel function, $\mu', \mu \in [-\pi, \pi)$ account for the mean direction of AoD and AoA respectively, and $\kappa', \kappa \geq 0$ control the angular spreads of AoD and AoA, respectively. Eq. (8) gives the final closed-form STCC function of the new two-ring model. Comparison of this model with measured indoor MIMO data is carried out in Section IV. For indoors, due to the low mobility of the receiver, we set $f_d = 0$, which simplifies Eq. (8) significantly.

IV. Comparison of the model with data

We now apply the previously discussed correlation model in Eq. (8) to the data collected at Brigham Young University. Details of the measurement campaign and room layouts can be found in [10]. The MIMO channel was 10×10, with the same $\lambda/4$ element spacing at both the transmit and receive arrays.

Before computing the correlation matrix, some kind of normalization is necessary to remove the effect of path loss. In [11], the normalization is done according to $\frac{\sqrt{n'n}\mathbf{H}(l)}{\|\mathbf{H}(l)\|_F}$ for each l, where $\mathbf{H}(l)$ is a snapshot of the 10×10 channel matrix at time instant l, and n and n' are the number of MS and BS elements, respectively, and $\|\cdot\|_F$ is the Frobenius norm. In [12], normalization is done to guarantee the so-called single-input single-output (SISO) gain

$$L^{-1}\sum_{l=1}^{L} \| \mathbf{H}(l) \|_F^2 = n'n, \tag{9}$$

where L is the total number of snapshots available. These methods can not guarantee equal unit power for each sub-channel, which we need to compare our model in (8) with data. In this paper, the normalization is done on a subchannel by subchannel basis such that each subchannel has zero mean and unit variance, i.e., $\frac{h_{ij(l)} - m_{ij}}{\sigma_{ij}}$, where m_{ij} and σ_{ij}^2 are the mean and variance of the ijth subchannel, calculated from $\{h_{ij}(l)\}_{l=1}^{L}$.

A. Correlation

Here we consider four different correlations, i.e., parallel, crossing, transmit and receive correlations, defined by the

following equations:

$$\begin{aligned}\rho_{parallel}(\tau)&\triangleq E[h_{lp}(t)h^*_{(l+n)(p+n)}(t+\tau)]\\ \rho_{crossing}(\tau)&\triangleq E[h_{lp}(t)h^*_{pl}(t+\tau)]\\ \rho_{Tx}(\tau)&\triangleq E[h_{lp}(t)h^*_{lq}(t+\tau)]\\ \rho_{Rx}(\tau)&\triangleq E[h_{lp}(t)h^*_{mp}(t+\tau)].\end{aligned} \quad (10)$$

These correlations have been estimated from the data, for each possible antenna spacing, over all possible antenna elements. The correlation values obtained are then averaged over all the relevant data sets for different locations. For data collected on 11/07/00, there are 24 locations, 20 sets per location, and 124 snapshots of the 10×10 channel matrix per set; For 11/08/00, we consider the first 3 locations, 63 sets totally, and 124 snapshots of the 10×10 channel matrix per set.

To estimate the parameters of the new model, $\Lambda = (\Delta, \Delta', \kappa, \kappa', \mu, \mu', \eta)$, the channel correlation matrix, defined by

$$\mathbf{R_H} = E[\mathrm{vec}(\mathbf{H})(\mathrm{vec}(\mathbf{H}))^H], \quad (11)$$

needs to be estimated, where $(\cdot)^H$ is the complex conjugate transpose and $\mathrm{vec}(\cdot)$ is a column vector constructed by stacking the columns of its matrix argument. The parameter vector Λ is then estimated via a numerical least-square search, i.e., $\min_\Lambda \|\hat{\mathbf{R}}_\mathbf{H} - \mathbf{R_H}(\Lambda)\|_F$, in which $\hat{\mathbf{R}}_\mathbf{H}$ is the estimate of the correlation matrix, whereas $\mathbf{R_H}(\Lambda)$ is constructed according to Eq. (8). For 11/07/00 and 11/08/00, the estimated parameters are $\hat{\Lambda} = (\pi/3, \pi/6, 0, 0.5, 0, 5\pi/8, 0.2)$ and $\hat{\Lambda} = (\pi/3, \pi/6, 0, 0, \pi, 0, 0.2)$, respectively. Note that the directions of transmit and receive arrays are determined from room layouts, which are $\alpha = 168^o$ and $\beta = 78^o$, respectively. They are same for 11/07/00 and 11/08/00 due to the same room layout.

As shown in Fig. 3 and 4, the two-ring model provides a good match to all kinds of correlations defined in Eq. (10).

B. Channel Capacity

Assume that $\mathbf{H}$ is known at the receiver but not at the transmitter. If the total finite transmitted BS power, $P_{BS_{total}}$, is allocated uniformly to all the n' antennas of the BS array , then the capacity of the MIMO channel, in bits/s/Hz, is given by [1]

$$C/W = \log_2\left(\det\left(\mathbf{I}_n + \frac{P_{BS_{total}}}{n' P_{noise}}\mathbf{H}\mathbf{H}^H\right)\right), \quad (12)$$

where $\det(\cdot)$ is the determinant and P_{noise} is the noise power at each receive element. Note that the capacity in Eq. (12) is a random variable whose distribution depends on the distribution of the random complex matrix $\mathbf{H}\mathbf{H}^H$.

In literature, the SNR, which is equal to $P_{BS_{total}}/P_{noise}$, is usually assumed to take any value between 10 dB and 20 dB and is kept constant for all capacity calculations. This way, the effect of SNR only appears as a scaling factor for all the curves. Obviously, higher values for SNR mean higher capacities. For the collected data available, SNR was found to be close to 30 dB. For consistency with other capacity curves, widely found in literature, we chose SNR=20dB.

In the Fig. 3 and 6, which correspond 11/07/00 and 11/08/00 respectively, four capacity distributions are shown. The "Empirical" capacity distribution has been calculated according to Eq. (12), using the collected snapshots of $\mathbf{H}$. However, the "Two-ring model" and "Empirical Corr. Matrix" capacity distributions have been obtained by first coloring a simulated white Gaussian vector, i.e., left multiplying $\mathrm{vec}(\mathbf{H}_{iid})$ by the Cholesky factors $\mathbf{R}_\mathbf{H}^{1/2}(\hat{\Lambda})$ and $\hat{\mathbf{R}}_\mathbf{H}^{1/2}$, respectively, and then inserting it into (12). Obviously the "IID" capacity distribution has been obtained via inserting the simulated $\mathbf{H}_{iid}$ into (12).

From Fig. 3 and 6, one can conclude that the capacity predicted by our parametric model, is almost the same as the capacity predicted by the empirical channel correlation matrix. However, our model characterizes the channel with few physical parameters, whereas the empirical channel correlation matrix, which is a 100×100 matrix, does not provide, directly, information about the channel structure and physical parameters of interests such as the mean AoD and AoA, angle spreads, etc. Obviously, a system designer can easily study the effect of different channel parameters on the capacity , using our parametric model.

Interestingly, there is a gap between the "Empirical" capacity distribution and the other two distributions. This probably could be improved by using a proper complex non-Gaussian model for the channel matrix $\mathbf{H}$.

V. Conclusion

In this contribution a novel parametric model for indoor MIMO channels is proposed. This model yields a closed-form and mathematically tractable expression for the spatio-temporal cross-correlation among the subchannels, in terms of few physical parameters that characterize the indoor channel. Comparison of this correlation model with the indoor MIMO data has demonstrated the utility of the model in describing real data. The theoretical results of this paper, supported by empirical observations, provide useful tools and guidelines for efficient design of indoor multi-antenna transmission systems.

References

[1] G. J. Foschini and M. J. Gans, "On limits of wireless communications in a fading environment," *Wireless Personal Commun.*, vol. 6, pp. 311–335, 1998.

[2] H. Özcelik, M. Herdin, W. Weichselberger, J. Wallace, and E. Bonek, "Deficiencies of 'kronecker' MIMO radio channel model," *Electron. Lett.*, vol. 39, pp. 1209–1210, 2003.

[3] T. Svantesson and J. W. Wallace, "Tests for assessing multivariate, normality and the covariance structure of mimo data," in *Proc. IEEE Int. Conf. Acoust., Speech, Signal Processing*, 2003, pp. 656–659.

[4] A. Abdi and M. Kaveh, "A space-time correlation model for multielement antenna systems in mobile fading channels," *IEEE J. Select. Areas Commun.*, vol. 20, pp. 550–560, 2002.

[5] J. W. Wallace and M. A. Jensen, "Measured characteristics of the MIMO wireless channel," in *Proc. IEEE Vehic. Technol. Conf.*, Atlantic City, NJ, 2001, pp. 2038–2042.

[6] K. Yu and B. Ottersen, "Models for MIMO propagation channels, a review," *Wirel. Commun. Mob. Comput.*, vol. 2, pp. 653–666, 2002.

[7] G. J. Byers and F. Takawira, "The influence of spatial and temporal correlation on the capacity of MIMO channels," in *Proc. IEEE Wireless Commun. Networking Conf.*, Orleans, LA, 2003, pp. 359–364.

[8] W. Honcharenko, H. L. Bertoni, and D. L. Dailing, "Bilateral averaging over receiving and transmitting areas for accurate measurements of sector average signal strength inside buildings," *IEEE Trans. Antennas Propagat.*, vol. 43, pp. 508–512, 1995.

[9] W. C. Jakes, Ed., *Microwave Mobile Communications*. New York: Wiley, 1974.

[10] J. W. Wallace, "Modeling electromagnetic wave propagation in electrically large structures," Ph.D. dissertation, Brigham Young Univ., Provo, UT, 2002.

[11] J. W. Wallace and M. A. Jensen, "Modeling the indoor MIMO wireless channel," *IEEE Trans. Antennas Propagat.*, vol. 50, pp. 591–599, 2002.

[12] K. Yu *et al.*, "Second order statistics of NLOS indoor MIMO channels based on 5.2 GHz measurements," in *Proc. IEEE Global Telecommun. Conf.*, San Antonio, TX, 2001, pp. 156–160.

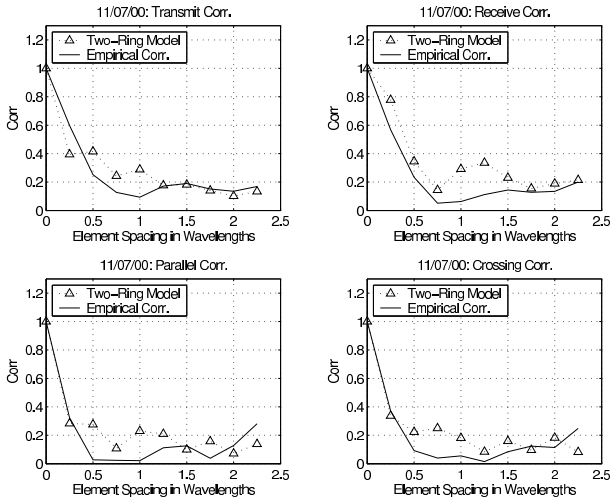

Fig. 3. Comparison of the new MIMO model with empirical correlations (11/07/00 data)

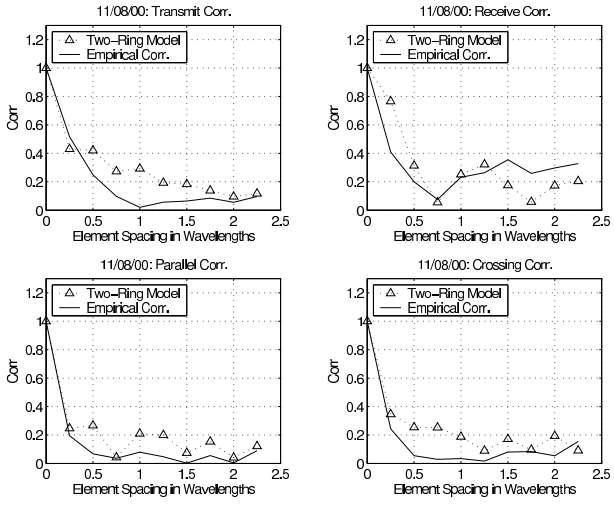

Fig. 4. Comparison of the new MIMO model with empirical correlations (11/08/00 data)

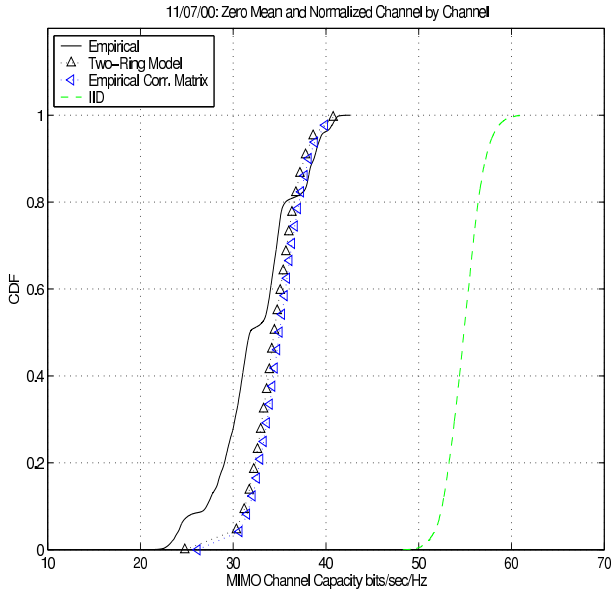

Fig. 5. Comparison of the new MIMO model with empirical capacity (11/07/00 data)

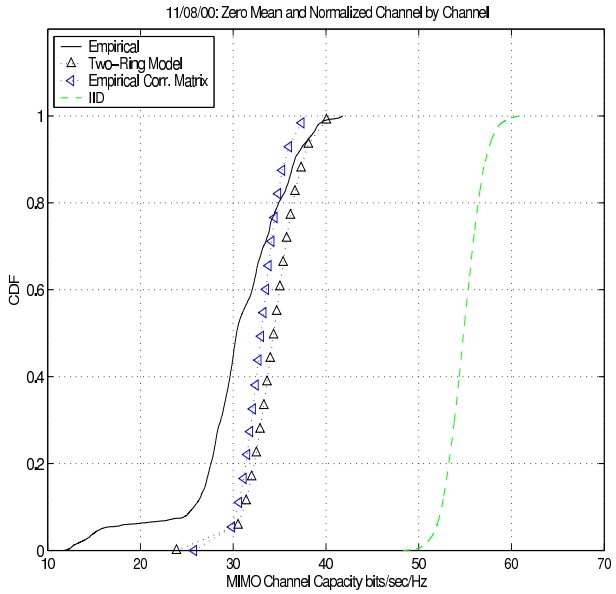

Fig. 6. Comparison of the new MIMO model with empirical capacity (11/08/00 data)